buildings

MDPI

Article

Flexural Behavior and Sustainability of Dual-Waste Fiber-Reinforced Concrete Designed for Pavement Applications

Mehmet Tevfik Seferoğlu *, Yavuz Selim Aksüt and Ayşegül Güneş Seferoğlu

Department of Civil Engineering, Gümüşhane University, Gümüşhane 29000, Türkiye; yselimaksut@gumushane.edu.tr (Y.S.A.); gnskaya61@gumushane.edu.tr (A.G.S.)
* Correspondence: mtseferoglu@gmail.com; Tel.: +90-4562331000

Abstract

This study evaluates the mechanical performance and sustainability potential of fiber-reinforced concrete incorporating mine tailings as the fine aggregate and waste tire wire as the reinforcing fiber. The concrete mixtures contained 0.2%, 0.4%, and 0.6% waste tire wire with the natural fine aggregate replaced entirely with Pb-Zn-Cu tailings. The mixtures were tested for porosity, water absorption, compressive strength, splitting tensile strength, flexural strength, toughness, fracture energy, and ductility to assess their mechanical performance and durability. The mine tailings improved the microstructure and reduced water absorption, particularly with tire wire. Using waste tire wire improved the compressive, tensile, and flexural performance; in particular, W-6 showed a 18.2% rise in compressive strength and a more than twofold increase in flexural strength relative to the control mix. The flexural toughness and fracture energy rose by up to 161%, while the ductility peaked at a fiber content of 0.2%. These gains were attributed to fiber crack-bridging and post-cracking energy absorption. The dual-waste system also reduced porosity, improved durability, and demonstrated strong potential for rigid pavement applications such as highways, industrial yards, and airport runways that require high fatigue resistance and a long service life. Beyond technical performance, this approach offers a sustainable solution that lowers maintenance, reduces life-cycle costs, and aligns with circular economy principles.

Keywords: alternative aggregates; fiber-reinforced concrete; mechanical properties; mine tailings; rigid pavement; sustainability

Academic Editors: Wenlin Tu and Shengqian Ruan

Received: 16 August 2025
Revised: 14 September 2025
Accepted: 22 September 2025
Published: 24 September 2025

Citation: Seferoğlu, M.T.; Aksüt, Y.S.; Seferoğlu, A.G. Flexural Behavior and Sustainability of Dual-Waste Fiber-Reinforced Concrete Designed for Pavement Applications. *Buildings* **2025**, *15*, 3454. https://doi.org/10.3390/buildings15193454

1. Introduction

In recent years, rigid pavements have gained prominence for their high durability and extended service life. The surge in concrete consumption across the world, given its primacy in construction, has accelerated resource drawdown and industrial waste accumulation [1]. Conventional concrete production depends heavily on virgin aggregates and steel reinforcement, both of which present notable environmental and economic drawbacks. Consequently, integrating waste-derived materials into concrete production has become an important strategy for mitigating ecological impacts and supports the conservation of natural resources. As the construction industry pursues global sustainability objectives, industrial by-product recycling and reuse are gaining recognition as crucial measures. Using such by-products in concrete reduces the reliance on natural aggregates while promoting cost-efficient, eco-friendly handling of waste. In this context, mining by-products, particularly residues from lead, zinc, and copper operations, can serve as alternative aggregates or binders, helping to address challenges such as heavy metal release, soil

degradation, and water contamination, while reducing the high disposal costs [2]. In this study, Pb-Zn-Cu tailings were chosen due to their regional abundance and large stockpiles and have significant reuse potential and sustainability benefits in concrete production [3]. The tailings in the 0–5 mm fraction were processed and employed as a fine aggregate to evaluate their mechanical performance and practical feasibility rather than exploiting any chemistry-specific reactivity. Despite these advantages, the direct application of mining wastes in pavement-grade concrete remains relatively underexplored in the existing body of research.

Mine tailings, a major by-product of the mining industry are typically disposed of in large quantities, occupying land and posing long-term ecological risks. Properly processed tailings can function as fine aggregate substitutes in concrete, with reports [4–8] indicating that they produced denser mixes and reduced water absorptivity. As the volumes of scrapped tires increase, excess tire wire becomes available and, due to its steel content and notable tensile strength, it can be deployed as a reinforcing material. Studies [9–13] have demonstrated that, compared with synthetic fibers, steel fibers (SFs) provide significant gains in flexural behavior and overall toughness. Additionally, the aggregate type strongly influences the concrete's compressive response and modulus of elasticity. Mindess et al. emphasized that both the mechanical and microstructural interactions between aggregates and the cementitious matrix affect the overall concrete performance, especially in high-strength concrete [14]. Studies rarely address the concurrent use of mine tailings and waste tire wire in concrete, especially the mutual enhancements they may provide in mechanical and sustainability outcomes.

While concrete is indispensable to contemporary infrastructure due to its compressive strength, durability, and ease of production, the processes of aggregate extraction and Portland cement manufacturing cause notable environmental impacts, including resource depletion, greenhouse gas emissions, and waste [15,16]. Contemporary studies have investigated the usage of waste streams from industry and mining as replacement materials in concrete to satisfy environmental and performance criteria. Interest in concrete made with industrial and post-consumer waste streams has risen, reflecting both environmental priorities and economic incentives. Among these, waste tire products including rubber particles and steel tire wires have been widely explored for their potential to improve energy absorption and post-crack behavior in concrete mixtures. Concurrently, the incorporation of mine tailings, particularly as a fine aggregate replacement, has shown promising results in enhancing mechanical strength and reducing the environmental footprint of concrete. These materials have been evaluated not only in general structural concrete applications but also in road pavement layers where durability and sustainability are critical performance metrics. Furthermore, "RubCrete", developed using recycled tire wire, exemplifies the potential of waste inputs to generate new, high-performance concrete systems (Table 1). However, studies on the waste tire wire fiber concretes containing mine tailings are still limited, as can be seen from Table 1.

Table 1. Studies on concretes produced using wastes (tire wire and mine tailings).

Reference	Waste Material(s) Used	Application	Material and Ratios	Key Findings
[17]	Waste rubber particles (coarse)	Concrete	5–30%, optimum: 10%	Strength decreases after 10%
[18]	Waste rubber aggregate	Concrete	Between 10 and 35%	Eco-friendly additive for non-structural concrete
[19]	Rubber particles + waste tire wire	Concrete	10% rubber + 0.25% wire	Improved energy absorption and strength

Table 1. *Cont.*

Reference	Waste Material(s) Used	Application	Material and Ratios	Key Findings
[20]	Mine tailings + SF	Concrete	10–20%	10% is optimal for strength enhancement
[21]	Iron ore tailings (fine aggregate)	Pavement	Between 20 and 50%	Positive effect on performance, sustainable solution
[22]	Iron ore tailings	Concrete	0–25%	Increased strength, decreased workability
[23]	Iron tailings + SF/basalt fiber	Concrete	Between 10 and 30%	Performance enhanced with fiber
[24]	Graphite tailings	Asphalt	Up to 50%	Improved performance, economic benefits
[25]	Tire wire + concrete	Concrete	Applied as "RubCrete"	Tough and eco-friendly concrete

Mine tailings, which are produced as fine by-products of metallic ore operations, pose notable environmental hazards in the absence of appropriate management. Studies have shown that partial replacement of natural fine aggregates with mine tailings can reduce porosity and water absorption while increasing the density and compressive strength of concrete, particularly when the tailings are processed appropriately. Moreover, investigations on Pb-Zn-Cu (lead–zinc–copper) mine tailings in pavement applications demonstrated improved early-age moduli of elasticity and mechanical performances when combined with supplementary reinforcements. Parallel to this, recycled SFs recovered from end-of-life vehicle tires have emerged as promising alternatives to manufactured SFs for use in fiber-reinforced concrete (FRC). These recycled fibers not only reduce the volume of solid waste, but also enhance the post-cracking behavior, flexural strength, and fracture energy of cementitious composites [10,26,27]. Research has consistently shown that at optimized dosages (typically 0.2–0.6% by volume), recycled tire SFs can significantly improve concrete toughness and elastic modulus without compromising workability, especially in lightweight or pavement-grade concretes. Additionally, the hybridization of recycled tire SFs with other industrial fibers has been found to synergistically improve the crack-bridging ability and matrix integrity. Fares et al. reported that a hybrid mixture with 0.5% industrial steel fibers and 0.5% recycled tire fibers produced a 31.7% increase in compressive strength and an 8.14% rise in elastic modulus relative to the control mixes [28]. Similarly, basalt FRCs have demonstrated substantial improvements in fracture energy and crack resistance, reinforcing the value of short-fiber reinforcement in geopolymeric or cementitious matrices. Even with recent advances, the co-utilization of mine tailings and waste tire SFs has received limited attention, particularly their combined effects on mechanical performance, durability, and sustainability indicators. Most existing studies focused on either alternative aggregates or fiber reinforcement independently, overlooking their potential interactions in the cement matrix. Consequently, there is a need for deeper studies to understand the integrated impact of these two types of waste materials on concrete properties, including strength development, elasticity, fracture resistance, and microstructural behavior.

In light of this gap, the mechanical response of fiber-reinforced concretes incorporating mine tailings as the fine aggregate and recycled tire steel fibers as the reinforcement was investigated. Mixtures were produced with fiber volume contents of 0.2%, 0.4%, and 0.6%, and the physical and mechanical characteristics were evaluated via compressive, splitting tensile, and elastic modulus tests. Unlike previous studies that considered mine tailings or recycled tire fibers separately, this work uniquely focuses on their combined use in a

single concrete system, emphasizing their synergistic effects on strength, durability, and sustainability. The novelty of this study lies in demonstrating the potential of Pb-Zn-Cu mine tailings and recycled tire SFs to deliver both enhanced mechanical performance and a sustainable material solution, particularly for pavement-grade applications. By examining the compressive and flexural behavior of these dual-waste concretes, this work advances eco-friendly, structurally efficient composites that curb the use of virgin resources and conform to circular economy principles.

2. Materials and Methods

2.1. Materials

2.1.1. Aggregates

In this study, mine tailings originating from Pb-Zn-Cu ores were used as the fine aggregate (0–5 mm) while a 5–25 mm limestone fraction was used as the coarse aggregate in the mixes. The rocks were subjected to washing and drying processes due to the presence of clay and silt in their surroundings and then crushed to concrete aggregate sizes using a jaw crusher. The processed materials were then sieved into 0–5 mm, 5–12 mm, and 12–25 mm size fractions. The equipment used for the crushing and sieving processes is shown in Figure 1.

Figure 1. Pb-Zn-Cu tailings and limestone aggregates obtained using jaw crusher and sieve analysis machine.

The aggregates' physical characteristics are listed in Table 2, and their chemical components are shown in Table 3.

Table 2. Physical characteristics of the aggregates.

Aggregate Type	Aggregate Grade (mm)	Physical Properties			
		Dry Grain Density (g/cm^3)	Saturated Dry Surface Density (g/cm^3)	Water Absorption (%)	Porosity (%)
Mine tailings	0–5	2.68	2.72	4.01	10.72
Limestone	5–12	2.70	2.81	4.22	10.61
	12–25	2.71	2.78	1.98	4.88

Table 3. Chemical components of the aggregates.

Aggregate Type	SiO_2	Al_2O_3	Fe_2O	MgO	CaO	$MgCO_3$	Zn	Pb	Cu	H_2O	Others (CO_2, etc.)	Total
Mine tailings	-	-	4.65	-	34.6	-	1.11	0.98	>0.01	7.96	50.68	100
Limestone	2.95	0.43	0.46	-	73.93	22.23	-	-	-	-	-	100

2.1.2. Cement

The concrete mixes used locally sourced CEM I 42.5 R cement; the physical and mechanical characteristics and chemical components are listed in Table 4.

Table 4. Physical, mechanical, and chemical characteristics of the cement.

Chemical Characteristics		Physical Characteristics	
	Mass Percentage in Cement (%)		**Mass Percentage in Cement (%)**
SiO_2	18.51	Insoluble residue	0.86
Al_2O_3	4.23	45 micron sieve residue	2
Fe_2O_3	3.38	90 micron sieve residue	0
CaO	60.46	Consistency water quantity	30.7
MgO	2.79	Initial setting time (min)	195 min
SO_3	3.11	Final setting time (min)	240 min
Loss of ignition	3.53	Specific mass	3.10 g/cm^3
Na_2O	0.33	Expansion (Le Chatelier)	1 mm
K_2O	0.74	Specific surface (Blaine)	3627 cm^2/g
Cl	0.0106	Mechanical properties	
		Time (day)	Strength (N/mm^2)
Total	97.42	1	13.1
Unmeasurable	2.58	2	28
Free lime	0.68	28	57.8

2.1.3. Steel Fibers (SFs) from Recycled Tires

SFs were sourced from discarded tires through a mechanical fragmentation procedure. Their diameters were determined using an electronic caliper. The fiber lengths were not uniform due to the nature of the mechanical fragmentation and are therefore presented as a range. The fibers' aspect ratio was calculated by dividing their length by their diameter. Representative images of the SFs are displayed in Figure 2 while their physical characteristics are listed in Table 5. As shown in Figure 2, the SFs exhibited a curled morphology and displayed variability in both length and diameter.

Figure 2. The SFs from waste vehicle tires.

Table 5. The physical properties of the SFs.

SF	Diameter (mm)	Length (mm)	Aspect Ratio (%)	Weight Ratio (%)
	0.10–0.15	15–35	110–180	40–60

It is well established that the fiber volume fraction (V_f) has a direct effect on the workability of concrete. It is widely reported that the appropriate V_f for concrete mixtures falls in the 0.5–2.5% range [29–31]. However, it has also been shown that higher fiber dosages within this range cause significant reductions in flowability; for example, with straight fibers at 1%, 2%, and 3%, the mix flowability dropped by 14.9%, 25.6%, and 38.1%, respectively [32]. In addition, since the mine tailings used in this study consisted of fine particles (0–5 mm), the workability would have been further aggravated at higher fiber contents. For this reason, in the present study, we intentionally adopted a lower dosage range of 0.2–0.6%, which is in line with the lower bound reported by prior studies and has also been found to optimize the mechanical benefits without compromising workability in recent research [28].

2.2. Methods

Concrete Mix and Sample Preparation

A standard concrete mix consisting entirely of basalt aggregates in three distinct particle size ranges (0–5 mm, 5–12 mm, and 12–25 mm) was prepared to serve as the control mix and was designated as "C". In this control mix, the natural aggregates in the 0–5 mm size range were replaced with Pb-Zn-Cu tailings of equivalent size, forming a new mix labeled as "W". Since only the fine aggregate fraction was replaced, recycled materials accounted for approximately 45% of the total mix weight. They were incorporated into the fresh mix to assess the potential of recycled SFs as a reinforcement in concrete. These recycled SFs, which were sourced from waste vehicle tires, were introduced into the W mix at volumetric proportions of 0.2%, 0.4%, and 0.6%, resulting in mixes designated as W-2, W-4, and W-6, respectively. In this way, concrete mixtures incorporating both mine tailings and recycled SFs were successfully produced. For each mixture, twelve cylinders were cast: six were cured for 7 days and six for 28 days. Additionally, six prisms were prepared, with three cured for 7 days and three for 28 days. In total, sixty cylindrical and thirty prismatic concrete specimens were prepared for the C, W, W-2, W-4, and W-6 mixtures (Figure 3) and water-cured until the tests were performed.

Three out of the six cylindrical specimens from each mixture group were initially non-destructively tested for physical properties including porosity and void ratio. Splitting tensile tests were then performed on these specimens. The other three specimens were reserved for compression tests, enabling the calculation of the modulus of elasticity and Poisson's ratio. Additionally, the flexural strength was measured on 10 × 10 × 40 cm prismatic samples and the obtained data (Figure 4) were used to evaluate the tensile strength in bending and additional bending-related properties.

The results for each test category were evaluated using the mean of three companion specimens. The mix proportions for the recycled SF–reinforced concretes are listed in Table 6.

The fibers were pre-weighed for each batch and introduced gradually into the fresh mix to avoid balling. The mixing protocol was as follows: (i) dry blending of aggregates and cement, (ii) addition of water + SP, and (iii) slow sprinkling of the recycled tire steel fibers over 60–90 s while mixing at low speed followed by 60–90 s at a higher speed with intermittent wall scraping. During casting, no fiber clumps were observed; the molds were filled in two lifts with light rodding to minimize segregation. As a post-casting qualitative

check, representative specimens were inspected after demolding and after mechanical testing (fracture planes of flexural beams); uniformly dispersed fibers bridging the cracks were observed without evidence of balling or settlement. The batch fiber masses matched the target dosages (Table 6) and were recorded to verify the dosing accuracy.

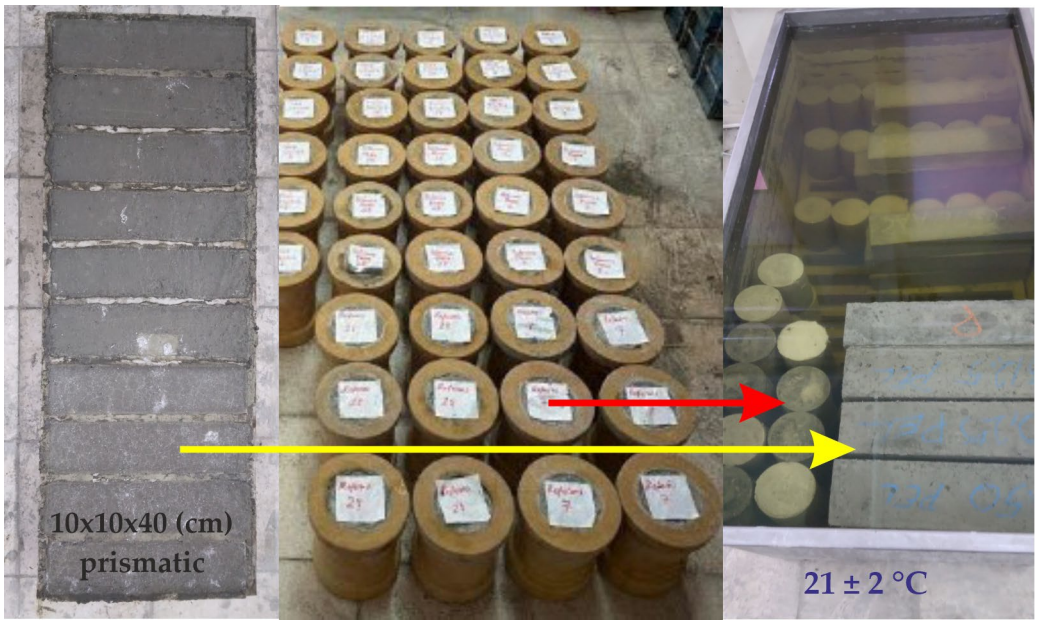

Figure 3. Concrete samples used in the study.

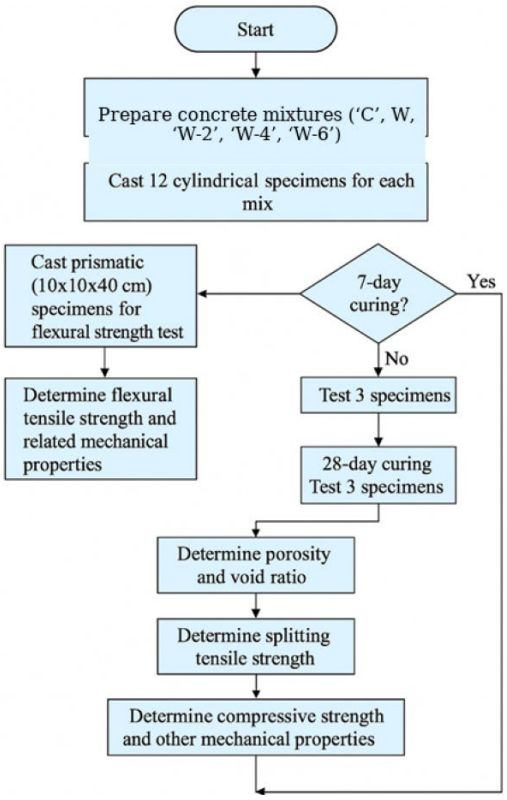

Figure 4. Production steps for concrete mix.

Table 6. Mix proportions of recycled SF-reinforced concrete.

Mix code	Cement (kg/m^3)	Water (L/m^3)	Aggregate (kg/m^3)	SP (kg/m^3)	Pb-Zn-Cu Tailings (0–5 mm) (kg/m^3)	SFs	
						(%)	(kg/m^3)
C	350	175	1744.03	5.25	-	-	-
W	350	175	1744.03	5.25	784.81	-	-
W-2	350	175	1744.03	5.25	784.81	0.2	15.7
W-4	350	175	1744.03	5.25	784.81	0.4	31.4
W-6	350	175	1744.03	5.25	784.81	0.6	47.1

2.3. Test Procedures

2.3.1. Physical Characteristics

Three specimens were selected from each concrete group incorporating different fiber ratios and their physical properties were tested according to the ASTM C642 standard [33]. Initially, the samples were cured in temperature-controlled water at 23 ± 2 °C until full saturation was achieved. Following saturation, the specimens were taken out and the surface moisture was carefully removed before their mass in air was recorded. Subsequently, their submerged mass was determined using the Archimedes principle. Finally, the specimens were oven-dried at 105 °C, allowed to cool to room temperature, and then weighed to obtain their dry mass. The density, void ratio, and water absorption were subsequently computed using Equations (1), (2), and (3), respectively.

The density was calculated using the determined mass and volume of the sample using the equation given below:

$$D = \frac{M}{V} \quad (1)$$

where

D: The density of the specimen depending on its moisture condition and the volume determination method (kg/m^3);

M: The mass of the specimen based on its condition during testing (kg);

V: The volume of the specimen determined using a specific method (m^3).

The water absorption of the specimens and the porosity values calculated based on these amounts were determined using the relevant formulas provided in the standard (Equations (2) and (3)).

$$P = \frac{W_{DA} - W_{KA}}{V_N} * 100 \quad (2)$$

where

P: Visible void ratio (%);

W_{DA}: Weight of saturated dry surface material (kg);

W_{KA}: Dry weight of sample (kg);

V_N: Sample volume (dm^3).

The water absorption rate was calculated as follows:

$$W_a = \frac{W_{DA} - W_{KA}}{W_{KA}} * 100 \quad (3)$$

where

W_a: The water absorption based on mass (%);

W_{KA}: The dry weight of the sample (g);

W_{DA}: The weight of the saturated dry surface material (g).

2.3.2. Mechanical Characteristics

Following BS EN 12390-3 [34], the compressive strength was determined at curing ages of 7 and 28 days. Uniaxial compressive strength tests were applied to control mix and FRC standard cylindrical specimens measuring 100 × 200 mm. The tests were performed at a constant loading rate of 0.6 ± 0.2 MPa/s. The compressive strength was calculated from three cylinders per mix using Equation (4). The elastic modulus and Poisson's ratio were evaluated as per ASTM C39 [35]. The modulus of elasticity was determined using Equation (5). The axial and lateral strains were measured during testing using extensometers attached to a gauge that captured changes in both length and diameter. Poisson's ratio was obtained from the lateral strain/axial strain using Equation (6).

$$F_C = \frac{F}{A_C} \quad (4)$$

where

F_c: Compressive strength (MPa);

F: Maximum load reached at fracture (N);

A_C: Cross-sectional area of the specimen on which the compressive load was applied (mm^2).

$$E = \frac{\sigma}{\varepsilon} \quad (5)$$

where

E: Modulus of elasticity (MPa);

σ: Stress (MPa);

ε: Strain.

$$v = \frac{\varepsilon_{lateral}}{\varepsilon_{axial}} \quad (6)$$

where

v: Poisson's ratio (%);

$\varepsilon_{lateral}$: Lateral strain;

ε_{axial}: Axial strain.

The splitting tensile strength was measured at 7 and 28 days as per ASTM C496 [36] to assess the influence of the fibers on tensile behavior. The tests were conducted on cylindrical specimens (with identical dimensions to those used for compression testing) using a material testing system under strain-controlled loading. Using a constant rate of 0.04–0.06 $N/mm^2 \cdot s$, the test recorded the maximum load at failure; the strength in splitting tension was then obtained using Equation (7). For each mix, the reported value is the average of three specimens.

$$T = \frac{2P}{\pi DL} \quad (7)$$

where

T: Splitting tensile strength (MPa);

P: Peak load at failure point (N);

D: Diameter of the cylinder (mm);

L: Length of the cylinder (mm).

Shear and flexural internal forces frequently act simultaneously in structural concrete elements such as beams and slabs. Flexural forces are generated by member bending, while shear forces result from the relative sliding between adjacent concrete sections. Assessing concrete specimens under such combined loading conditions enables a better understanding of their mechanical behavior and allows for a more accurate determination of their strength and long-term durability in practical applications. Safe and effective performance demands that both the flexural and shear capacities be included in the structural design and

analysis process. Fundamentally, the distinction between pure and non-pure bending lies in the type of internal stresses generated by the applied loads. Impure bending encompasses both bending and shear effects while pure bending considers only bending-induced stresses. As a result, the recorded strength corresponds to the genuine structural capacity of the material under defined, and often multi-axial, loading scenarios. The system automatically acquires deflection across the beam span, after which, it calculates the first peak (f_1) and peak flexural strengths (f_p) using Equations (8) and (9), respectively.

$$f_1 = \frac{P_1 L}{bd^2} \tag{8}$$

$$f_p = \frac{P_p L}{bd^2} \tag{9}$$

where

L: The span length (mm);
b: The average width of the specimen (mm);
d: The average depth of the specimen (mm);
P_1: The first-peak load (N);
P_p: The peak load (N).

The first-peak load P_1 (kN) is defined as the maximum load at the point of initial cracking on the load–deflection curve, as specified in ASTM C1609 [37]. The valley load after the first peak P_{val} (kN) is the local minimum load immediately after P_1 and before any subsequent hardening/second peak. The load drop magnitude is

$$\Delta P_{drop} = P_1 - P_{val}(kN) \tag{10}$$

and the load drop percentage is

$$\%Drop = \frac{P_1 - P_{val}}{P_1} \times 100(\%) \tag{11}$$

All loads are reported in kN and deflections are reported in mm.

Flexural toughness $U_{0\to L/150}$ is computed as the area under the load–deflection curve from zero deflection to the net deflection $L/150$ using trapezoidal numerical integration as per ASTM C1609 [33]. The area has units of kN·mm with the load in kN and deflection in mm; since 1 kN·mm = 1 J, we report the toughness directly in Joules (*J*). Thus,

$$U_{0\to L/150} = \int_0^{L/150} P(\delta)d\delta [J] \tag{12}$$

For clarity, in this paper, "energy absorption" refers to $U_{0\to L/150}$. "Fracture energy (G_f)" (Section 2.3.2) is reported separately in N/m and should not be conflated with toughness. Toughness indices serve as key parameters for characterizing the flexural capacity of fiber-reinforced composite beams, as they reflect the beams' capacity to absorb energy under loading. As defined in ASTM C1609 [37], flexural toughness is the area beneath the load–deflection response up to $L/150$. By numerically integrating the experimental curve to the required limit, the value was determined (Figure 5).

In addition, the equivalent flexural strength ratio was obtained from Equation (13), and the modulus of rupture (MOR) was derived from the maximum load via Equation (14).

$$R^D_{T.150} = \frac{150T^D_{150}}{f_1 bh^2} * 100 \tag{13}$$

where

T_{150}^{D}: The area under the load–deflection curve for deflections from 0 to L/150 (N·mm);
f_1: The first peak strength (MPa);
L: The span length (mm);
b: The average width of the specimen (mm);
h: The average depth of the specimen (mm);
P: The initial cracking flexural load (N).

$$MOR = \frac{P_p L}{bd^2} \tag{14}$$

where

P_p: Peak load at failure point (N);
L: Span length (mm);
b: Width of specimens (mm);
d: Depth of specimens (mm).

The G_f is the average energy required per unit area to induce failure in a material subjected to bending. This parameter quantifies the damage resistance under flexural loading. The formulation of this definition is presented in Equation (15).

$$G_f = \frac{W_0 - Wg\delta_0}{A_{lig}} \tag{15}$$

where

G_f: Fracture energy (N/m);
W_0: Area under the load–deflection curve (Nm);
W: Beam weight (kg);
g: Gravity acceleration (m/s^2);
δ_0: Deformation of the beam during fracture (m);
A_{lig}: Effective cross-sectional area (m^2).

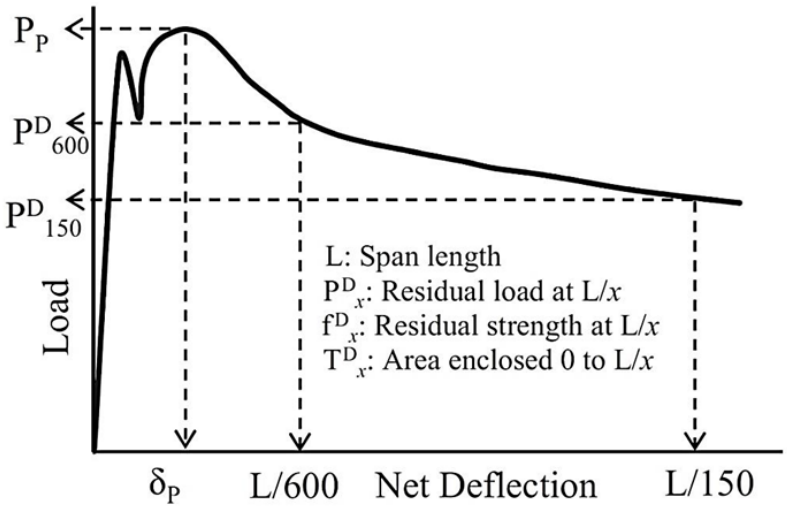

Figure 5. Typical load–deflection graph and toughness parameters [37–39].

The ductility index characterizes how long a concrete element can deform before breaking, with higher DI values reflect greater crack tolerance; it is calculated using Equation (16).

$$DI = \frac{G_f}{P_{max}} \tag{16}$$

where

DI: Ductility index (m^{-1});
G_f : Fracture energy (N/m);
P_{max}: Maximum load (kN).

Note that 1 kN·mm = 1 J; thus, the integrated area is in Joules, which is divided by the crack ligament area (m^2), giving G_f in J/m^2 = N/m.

3. Results and Discussion

3.1. Physical Properties

The use of mine tailings as the fine aggregate and waste tire wires as the fiber reinforcement in fiber-reinforced concrete provides both functional performance and sustainability benefits. Incorporating mine tailings in the fine fraction was particularly influential for durability as it affected key parameters such as porosity and water absorption. Prior studies indicated that the addition of mineral waste can lower porosity and refine the microstructure, which in turn enhances the overall durability [40,41]. Likewise, the inclusion of scrap tire wires at varying ratios (0.2%, 0.4%, and 0.6%) not only enhanced the mechanical strength through improving the fiber effect, but also contributed to improved concrete long-term service performance. Fiber reinforcement is known to limit microcrack propagation and thus reduce the ingress of aggressive agents. This dual contribution of mineral and fiber-based waste materials supports the development of more durable and sustainable concrete composites [42–44]. Figure 6 summarizes the 7- and 28-day porosity and water-absorption values of the control (C) and the FRC mixes.

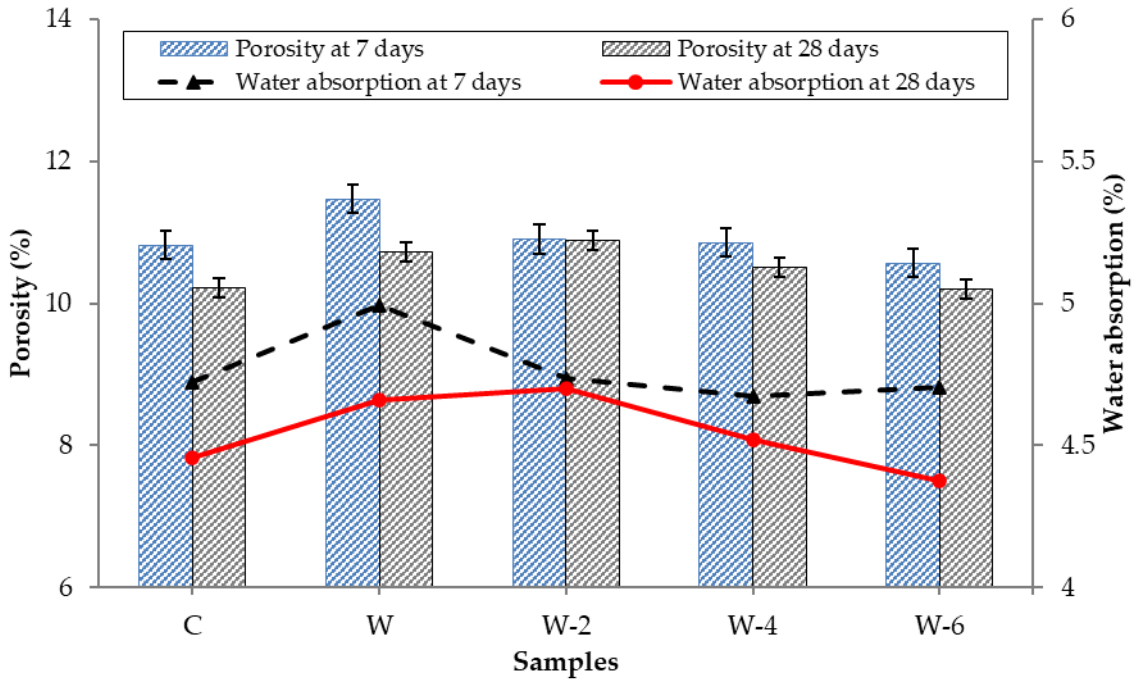

Figure 6. Porosity and water-absorption comparison of C and FRC mixes.

As illustrated in Figure 6, the porosity and water absorption values exhibited relatively stable behaviors across the different sample groups at 7 and 28days of curing. After 7 days, the porosity of the C mix was ≈10.8%, with a water absorption of ≈4.8%. Using mine tailings (W) as a fine aggregate substitute, the porosity increased to 11.8%, indicating a 9.3% rise, whereas the water absorption slightly increased to 5.0%, suggesting limited microstructural refinement at early curing ages.

Incorporation of 0.2% tire wire (W-2) caused a modest reduction in porosity to 11.0% (6.8% decrease compared to W) and a marginal decrease in water absorption. Similarly, the

W-4 and W-6 tire wire samples exhibited further decreases in porosity (10.7% and 10.4%, respectively), corresponding to a 9.5% total reduction for W-6compared to W. The water absorption in these samples remained nearly unchanged, fluctuating between 4.7 and 4.8% and implying that the addition of the fibers stabilized the permeability properties even at early ages. At 28 days, the porosity of all the mixtures declined due to the continued hydration and microstructural densification. The C mix reached 10.3% while the W series samples ranged from 11.0% (W) down to 10.1% (W-6). The water absorption values followed a consistent decreasing trend: C (4.8%) → W (4.9%) → W-2 (4.8%) → W-4 (4.6%) → W-6 (4.4%). The W-6 sample exhibited the lowest porosity and water absorption at both curing ages, with an overall 11.5% reduction in water absorption compared to W at 28 days. These findings confirm that while the initial replacement of natural fine aggregate with mine tailings (W) may temporarily increase the porosity and water absorption, the subsequent addition of waste tire wire, particularly at 0.4% and 0.6%, effectively mitigates this effect and enhances the microstructural performance over time. This behavior suggests that the combination of mine tailings and fiber reinforcement promotes pore refinement and reduces permeability with extended curing, contributing to more durable concrete composites. Similar trends have also been reported in recent literature, where recycled SFs were shown to enhance the densification of the cement matrix and limit permeability-related deterioration [9,41]. The relationship of water absorption vs. porosity is plotted in Figure 7.

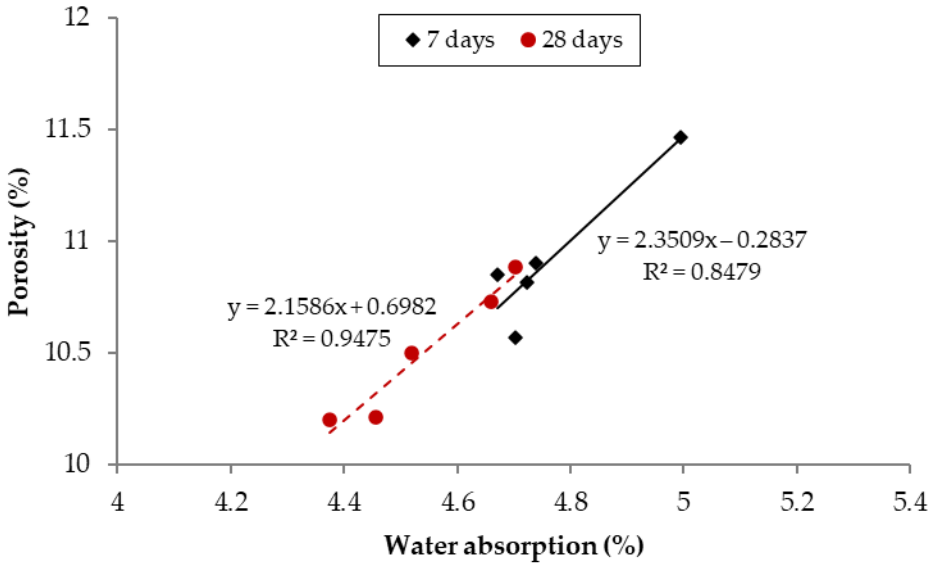

Figure 7. Correlation between porosity and water absorption in specimens.

Porosity and water absorption exhibited a high linear correlation for both curing ages, with R^2 values of 0.8479 at 7 days and 0.9475 at 28 days. The higher R^2 value at 28 days suggests a more consistent and compact microstructural development over time, indicating that water absorption is a reliable indicator of porosity, particularly at later curing stages.

The density values of all the mixtures ranged between 2392.97 and 2434.27 kg/m^3 at 7 days, which slightly increased at 28 days, with the highest value observed in the W-4 mixture (2431.02 kg/m^3) (Table 7). The porosity decreased from 10.82–11.47% at 7 days to 10.20–10.88% at 28 days, confirming progressive microstructural densification. Similarly, the water absorption values dropped from 4.72–4.99% at 7 days to as low as 4.37% in W-6 at 28 days, representing an overall reduction of about 7%. These results indicate that the combined use of mine tailings and waste tire wire contributed to a higher density and reduced permeability, thereby enhancing the durability of the composites.

Table 7. Density, porosity, and water absorption of specimens.

Sample	Density (kg/m^3)		Porosity (%)		Water Absorption (%)	
	7 Days	28 Days	7 Days	28 Days	7 Days	28 Days
C	2392.97	2398.68	10.82	10.21	4.72	4.46
W	2409.51	2410.99	11.47	10.73	4.99	4.66
W-2	2405.49	2426.97	10.90	10.88	4.74	4.70
W-4	2427.72	2431.02	10.85	10.50	4.67	4.52
W-6	2434.27	2352.71	10.57	10.20	4.70	4.37

3.2. Compressive Strength, Modulus of Elasticity, and Poisson's Ratio

The incorporation of waste tire wire into the concrete mixtures produced with mine tailings as the fine aggregate demonstrated variable influences on the mechanical performance (Table 8). The enhancement in compressive strength, particularly with lower fiber contents, could be due to the crack-bridging mechanism provided by the steel wires. Given their high tensile strength and strong adhesion within the matrix, the waste tire wires effectively delayed crack propagation, especially at the 0.2% replacement level, leading to a denser and more cohesive internal structure.

Table 8. Compressive strength, modulus of elasticity, and Poisson's ratio of specimens.

Sample	Compressive Strength (MPa)		Modulus of Elasticity (GPa)		Poisson's Ratio	
	7 Days	28 Days	7 Days	28 Days	7 Days	28 Days
C	18.58	21.99	27.49	47.80	0.29	0.30
W	15.03	18.00	31.02	44.50	0.31	0.33
W-2	21.47	22.87	37.44	72.80	0.31	0.34
W-4	22.96	24.21	30.84	33.30	0.33	0.37
W-6	22.44	26.00	26.64	29.69	0.34	0.41

As seen in Table 8, all the fiber-reinforced concrete samples incorporating waste tire wire and mine tailings as the fine aggregate showed higher compressive strengths compared to the control mix at 28 days. Specifically, the sample containing 0.2% tire wire (W-2) exhibited a 4.0% increase in strength compared to the control mix while the increase reached 10.1% and 18.2% for the W-4 (0.4%) and W-6 (0.6%) samples, respectively. These findings suggest that the addition of recycled SFs improves the mechanical integrity of the matrix, especially at higher fiber contents. However, the trend was not strictly linear as the strength gain at a lower fiber content (0.2%) was more modest, possibly due to insufficient fiber bridging. The improvements in compressive strength arise from the ability of tire wires to bridge microcracks and postpone their propagation. Such non-linear behavior aligns with the existing literature where the mechanical performance of fiber-reinforced concretes has been shown to vary based on fiber type, content, and dispersion efficiency [45–49].

The highest modulus of elasticity value was recorded in the W-2 sample (72.8 GPa), a substantial increase compared to the control mix (47.8 GPa). However, further increases in fiber content led to a decline in stiffness, with W-6 showing a value of 29.69 GPa. This reduction may be linked to the formation of weak zones or fiber agglomeration at higher dosages. The Poisson's ratio also followed a similar trend, increasing from 0.30 in the control mix to 0.41 in the W-6 mixture. This behavior indicates enhanced deformability due to an increased ductile response imparted by the waste tire wires. The results imply that the mechanical behavior of the fiber-reinforced mixtures is highly dependent on the fiber content and distribution within the matrix. It should be noted that while the modulus of elasticity reached its maximum at a fiber content of 0.2% (W-2), higher fiber dosages

(0.4–0.6%) resulted in a decline. This reduction is attributed to fiber agglomeration and the irregular geometry of recycled tire wires, which create weak zones and interrupt matrix continuity. Similar behavior has also been reported in the literature, which showed that recycled tire steel fibers enhanced stiffness at lower dosages but caused a decrease beyond the optimum threshold due to balling effects and heterogeneity [10,27].

It was noted that the Poisson's ratio of the W-6 mix (nearly 0.41) exceeded the typical 0.30–0.35 range for conventional concrete. This upward shift is consistent with the ductile response introduced by recycled tire steel fibers, which delay crack localization and promote higher lateral strain during loading (fiber-bridging and post-cracking deformability). Additionally, the Poisson's ratio of concrete is not constant; it can increase with damage evolution under compression. Differences in the C469 implementation (e.g., stress window, gauge length, and end-friction) may also contribute to higher measured values. These interpretations agree with recent reports on variable Poisson's ratios under loading and for fiber-reinforced concretes exhibiting increased lateral deformation [50–52].

3.3. Splitting Tensile Strength

In all the mixture types, the splitting tensile strength improved compared to the control, with the degree of increase dependent on the fiber ratio (Figure 8).

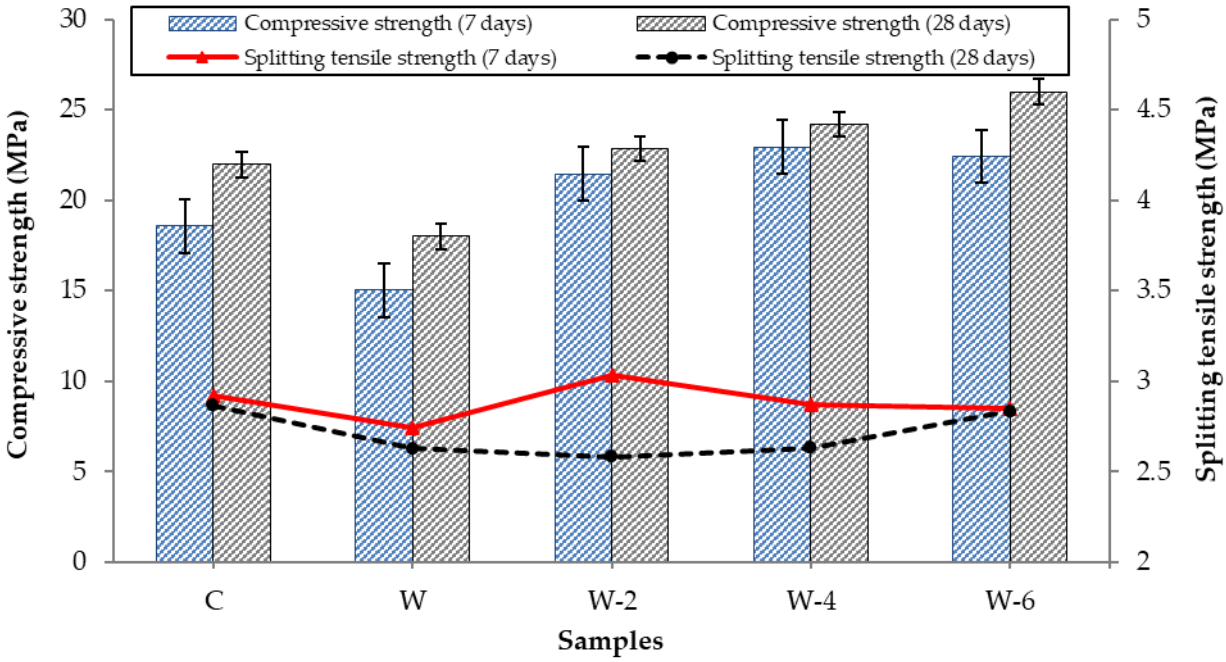

Figure 8. Splitting tensile strength according to fiber ratio and type.

The splitting tensile strength of the concrete mixtures varied significantly with curing time and the incorporation of waste tire wire, as shown in Figure 8. The control mix exhibited splitting tensile strengths of approximately 2.9 MPa at 7 days and 2.8 MPa at 28 days. In contrast, the mixture containing only mine tailings as the fine aggregate (W) showed slightly lower values of around 2.6 MPa (7 days) and 2.5 MPa (28 days), indicating a minor reduction in early- and later-age performance due to the replacement of the natural fine aggregate. However, the tensile strength increased to about 3.1 MPa at 7 days and 2.7 MPa at 28 days with the inclusion of 0.2% waste tire wire (W-2), showing a notable early-age improvement. Further increases in fiber content to 0.4% (W-4) and 0.6% (W-6) resulted in splitting tensile strengths of approximately 3.0 MPa and 2.9 MPa at 7 days and 2.8 MPa and 3.0 MPa at 28 days, respectively. The highest 28-day strength was observed in the W-6 mixture, representing a 7.1% increase compared to the control mix. These findings

indicate that the addition of fibers, particularly at higher contents, can effectively enhance both early- and later-age tensile performance likely due to the fiber effect of the recycled tire wires and the improved stress distribution within the matrix. The overall improvements are consistent with previous studies emphasizing the role of fiber type, dosage, and dispersion in optimizing tensile behavior in cementitious composites; however, the trend was not strictly linear. These results are consistent with findings from Zia et al. (2023) who reported a 15–25% increase in splitting tensile strength with increasing waste tire SF content in conventional concrete and from Gong et al. (2022) and Dziomdziora and Smarzewski (2025) who observed peak improvements in UHPC mixtures with a 1–2% fiber dosage [53–55]. In addition, the environmental benefits and mechanical compatibility of mine tailings as a fine aggregate are supported by circular economy principles, as discussed in recent reviews [56].

According to ACI 325 and EN 13877, pavement concretes should be evaluated against defined performance indices; EN 13877-1:2023 prescribes, among others, a compressive strength above 25 MPa and minimum flexural strength thresholds [57] while ACI 325.9R-15 emphasizes flexural performance as critical for a sufficient load-carrying capacity and long service life. In line with ACI guidelines, pavement concretes should achieve a 28-day flexural strength of 3.8–5.2 MPa and an elastic modulus of 28,000–41,000 MPa to ensure slab rigidity and effective stress transfer [58]. As summarized in Table 8 and shown in Figure 8, the test results indicate that only the W mixture does not satisfy these criteria, whereas the remaining mixes met—or in several cases exceeded—the relevant standard limits.

3.4. Flexural Strength, Toughness, and Modulus of Rupture

Beam performance was evaluated with respect to flexural strength, toughness, and ultimate capacity. Regression models were used to examine the impact of incorporating waste tire wire and varying fiber ratios on the flexural and splitting tensile responses (see Figure 9).

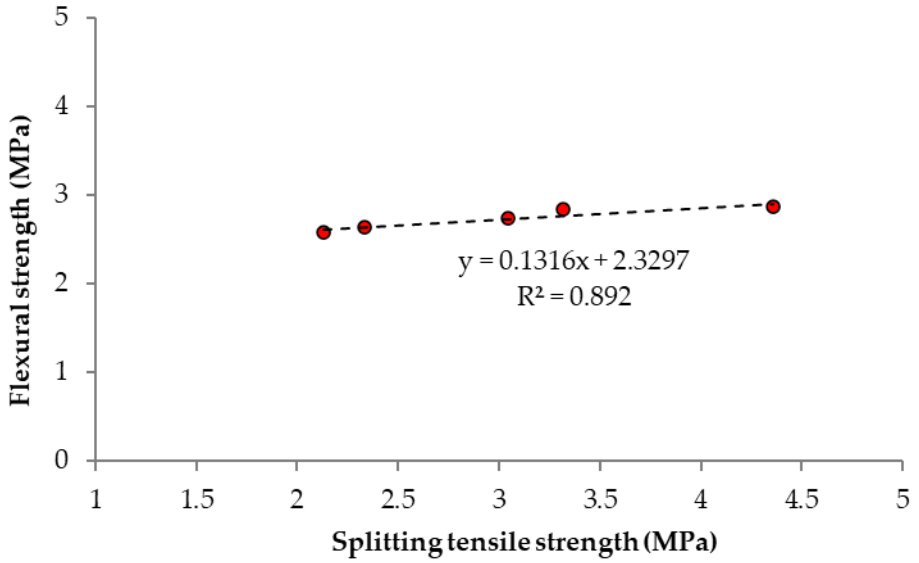

Figure 9. Relationship between flexural strength and splitting tensile strength of samples.

The relationship between the flexural strength and splitting tensile strength of the samples is shown in Figure 9. According to the regression equation y = 0.1316x + 2.3297 with a coefficient of determination R^2 = 0.892, there is a strong linear correlation between the two parameters. The flexural strength increased from 2.13 MPa to 4.36 MPa as the splitting tensile strength increased from 2.58 MPa to 2.87 MPa. This trend indicates that improvements in the tensile capacity of the matrix, possibly due to fiber bridging mechanisms, are positively reflected in its flexural performance [59–61].

Toughness—defined as the integral of the load-deflection (deformation) response—is widely considered a more dependable metric for capturing the effect of fibers in composites than conventional measures, such as compressive strength, flexural tensile strength, or modulus of rupture, from a mechanics standpoint [62,63]. Table 9 reports the first-peak load, second-peak load, and the percentage load drop for each concrete mixture. The gains observed in flexural performance are primarily ascribed to the fibers' crack-bridging action and the resulting improvement in load transfer across the cracked sections.

Table 9. Comparison of the first- and second-peak loads of the concretes.

Sample	First Peak, P_1	Valley After First Peak, P_{val}		Second Peak, P_p		Load Drop, ΔP_{drop}		Modulus of Rupture (MPa)
	kN	kN	%	kN	%	kN	%	
C	6.09	-	-	-	-	6.09	0	2.13
W	6.67	-	-	-	-	6.67	0	2.33
W-2	8.70	7.82	10.14	8.25	5.50	0.88	10.11	3.05
W-4	9.48	8.72	8.01	9.07	4.01	0.76	8.02	3.32
W-6	12.45	11.69	6.07	12.06	3.17	0.76	6.10	4.36

The mechanical performance of fiber-reinforced concretes can be significantly enhanced through the incorporation of SFs, particularly those derived from recycled sources. Table 8 demonstrates that as the waste tire wire content increases from 0.2% to 0.6%, both the first- and second-peak load values exhibited a substantial rise while the load drop percentage notably decreased. This trend indicates that the fiber effect contributes to a better post-cracking behavior and energy absorption capacity. The modulus of rupture also followed a similar pattern, reaching a 104% increase compared to the control mix. These results are consistent with recent findings in the literature. For instance, Maldar et al. observed notable improvements in the flexural and tensile performance of engineered cementitious composites reinforced with various SFs [64]. Likewise, a study on the flexural properties of fiber-reinforced concrete produced using hybrid SFs from waste tires reported significant enhancements in load-bearing capacity and post-peak behavior, further confirming the effectiveness of recycled SFs in improving the structural response of cement-based composites [65–67]. The flexural load-deflection behavior of the control mix, concrete with mine tailings as the fine aggregate (W), and fiber-reinforced concretes incorporating waste tire wire at 0.2% (W-2), 0.4% (W-4), and 0.6% (W-6) is presented in Figure 10.

The control mix exhibited a typical brittle failure behavior, with a maximum load of approximately 2.3 kN followed by a sharp drop in its load-carrying capacity. No significant post-crack resistance was observed and deflection was limited to around 1.8 mm. When mine tailings were used as the fine aggregate (W), the peak load increased to approximately 5.5 kN, indicating an improvement of about 139% compared to the control mix. However, a brittle post-peak behavior was still evident, with limited energy absorption and ductility. The inclusion of 0.2% waste tire wire (W-2) significantly enhanced the flexural performance with a peak load of about 10.7 kN, representing a 365% increase compared to the control mix. However, the post-peak load rapidly decreased, suggesting limited fiber bridging efficiency at this dosage. Both the peak load and ductility improved with a fiber content of 0.4% (W-4). The peak load reached approximately 9.8 kN, which is slightly lower than that of W-2, but the post-peak region exhibited a more gradual decline and extended deflection up to approximately 21 mm, indicating better energy dissipation. At a fiber content of 0.6% (W-6), the composite showed a lower peak load of about 3.6 kN but a distinct plateau-like post-crack region. The deflection extended to over 20 mm and the residual strength was maintained for a longer duration, reflecting improved toughness and

crack bridging despite a reduced peak strength. The present results align with those of prior studies showing that incorporating waste tire steel fibers markedly improves concrete toughness and post-cracking responses through crack-bridging mechanisms [68,69]. In addition, partially substituting natural fine aggregate with mine tailings has been reported to enhance flexural behavior and overall mechanical performance, primarily via denser particle packing and potential pozzolanic effects [70–72]. The ASTM C1609 parameters for the control mix and the FRCs with varying waste tire wire dosages are summarized in Table 10 [37].

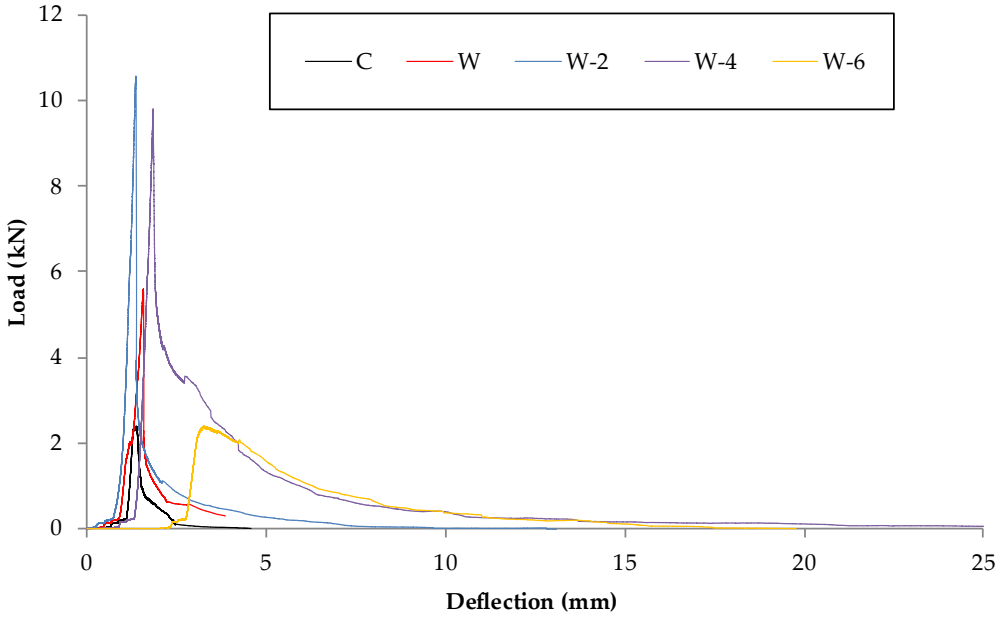

Figure 10. Typical flexural responses of FRCs compared to control mix.

Table 10. ASTM C1609 parameters for control mix and FRCs.

Sample	P_1 (kN)	f_1 (MPa)	Δ_1 (mm)	P_p (kN)	f_p (MPa)	Δ_p (mm)	P_{600}^{100} (kN)	f_{600}^{100} (MPa)	P_{150}^{100} (kN)	f_{150}^{100} (MPa)	$Toughness_{150}^{100}$ (J)	$R_{T,150}^{100}$ (%)	DI
C	6.09	2.13	0.9	6.09	2.13	1.1	3.96	1.39	1.86	0.65	36.36	17.31	1.22
W	6.67	2.33	1.03	6.67	2.33	1.08	5.27	1.84	3.59	1.26	53.65	24.73	1.68
W-2	8.7	3.05	1.18	8.25	2.89	1.35	7.41	2.59	5.88	2.06	84.05	33.62	1.99
W-4	9.48	3.32	1.4	9.07	3.17	1.77	8.36	2.93	7.4	2.59	90.33	32.26	1.84
W-6	12.45	4.36	1.85	12.06	4.22	2.26	11.02	3.86	9.84	3.44	94.99	29.41	1.45

P_1: first-peak load; f_1: first-peak strength; Δ_1: first-peak net deflection; P_p: peak load; f_p: peak strength; Δ_p: peak net deflection; P_{600}^{100}: load at L/600; f_{600}^{100}: strength at L/600; P_{150}^{100}: load at L/150; f_{150}^{100}: strength at L/150; $Toughness_{150}^{100}$: area under the load vs. net deflection curve from 0 to L/150; $R_{T,150}^{100}$ (%): equivalent flexural strength ratio; DI: ductility index.

The incorporation of mine tailings as the fine aggregate along with waste tire wire significantly enhanced the mechanical behavior of the concrete specimens according to ASTM C1609 flexural test results. The specimen with 0.6% waste tire wire (W-6) exhibited a 104.6% increase in first-crack strength and a 98.3% improvement in peak flexural strength compared to the control mix. Moreover, the toughness value increased by 152.9% while the

equivalent flexural strength ratio ($R^{100}_{T,150}$) showed a remarkable rise from 16.5% to 93.9%, highlighting a significant improvement in the post-cracking energy absorption capacity.

The DI also moderately improved, indicating an enhanced deformation capacity. These findings demonstrate that the combined use of mine tailings and waste tire wire fibers can substantially improve the flexural toughness and ductility of fiber-reinforced concrete. These results align with prior work showing that adding waste tire steel fibers markedly enhances concrete's flexural strength, toughness, and post-cracking response. Zeybek et al. reported that such fibers enhance both first-crack and peak flexural strength [13] while Aksoylu et al. confirmed notable improvements in energy absorption capacity and ductility when waste tire wire is combined with alternative aggregates such as mine tailings or recycled materials [68].

The post-peak response of W-4 was markedly more stable, leading to greater energy dissipation, although the representative load–deflection curves (Figure 10) show that W-2 reached a slightly higher peak load than W-4. Specifically, W-4 developed higher residual capacities at both L/600 and L/150 (8.36 vs. 7.41 kN and 7.40 vs. 5.88 kN, respectively), which resulted in a larger area under the curve (toughness of 90.33 J for W-4 vs. 84.05 J for W-2) (Table 10). This behavior indicates that the 0.4% dosage (W-4) mobilized a larger number of fibers in crack-bridging after the first peak while a 0.2% fiber dosage (W-2) can maximize the instantaneous peak by delaying the first crack and promoting stable crack growth, slower softening, and a higher residual strength. Mechanistically, the additional fibers engaged in pull-out at in the W-4 samples, increasing the post-cracking energy absorption even if the peak was not the highest. In contrast, the W-2 curve exhibited a narrower peak and a steeper post-peak drop, which is indicative of limited fiber engagement after the first crack. The quantitative consistency between the residual strengths (at L/600 and L/150) and the toughness ($U_{0\rightarrow L/150}$) substantiates this explanation.

Maximizing toughness requires an optimized fiber–matrix interface, which is controlled by interfacial adhesion, bearing (mechanical anchorage) resistance, the brittleness of the cementitious matrix, and the tensile capacity of the fibers. The relationships are plotted in Figure 11 (flexural toughness vs. equivalent flexural strength ratio) and Figure 12 (flexural toughness vs. modulus of rupture).

The flexural toughness of the specimens markedly improved with the incorporation of waste tire wire, as shown in the Figure 11. The toughness increased by approximately 47.6%, 131.2%, 148.5%, and 161.3% in the W, W-2, W-4, and W-6 samples compared to the control mix, respectively. The equivalent flexural strength ratio peaked in W-2 and slightly declined in the W-4 and W-6 samples, indicating a plateauing effect beyond a certain fiber threshold despite the consistent increase in toughness with an increasing fiber content. This behavior may be attributed to enhanced fiber effects and energy absorption at optimal fiber volumes, aligning with previous research findings [27,73,74].

As illustrated in the Figure 12, both the flexural toughness and modulus of rupture values exhibited a steady increase with the addition of waste tire wire into the mixtures. The W-6 sample demonstrated a significant enhancement of approximately 161% in flexural toughness and a 74% increase in modulus of rupture compared to the control mix. The modulus of rupture improved more gradually while the toughness values showed a sharp upward trend with increasing fiber content. This trend reflects the crack-bridging capability of the fibers, which becomes more effective at higher dosages, thereby improving energy absorption and delaying crack propagation. Similar enhancements in mechanical performance with increasing waste SF content have also been reported in recent studies [27,73,75].

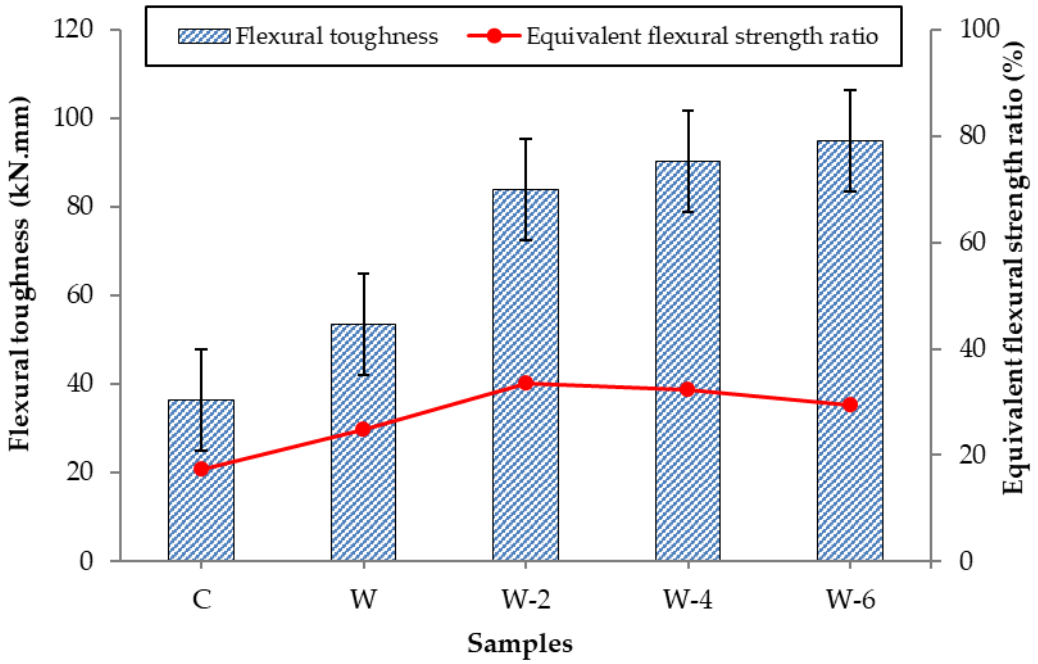

Figure 11. Dependence of equivalent flexural strength ratio on flexural toughness in control mix and FRCs.

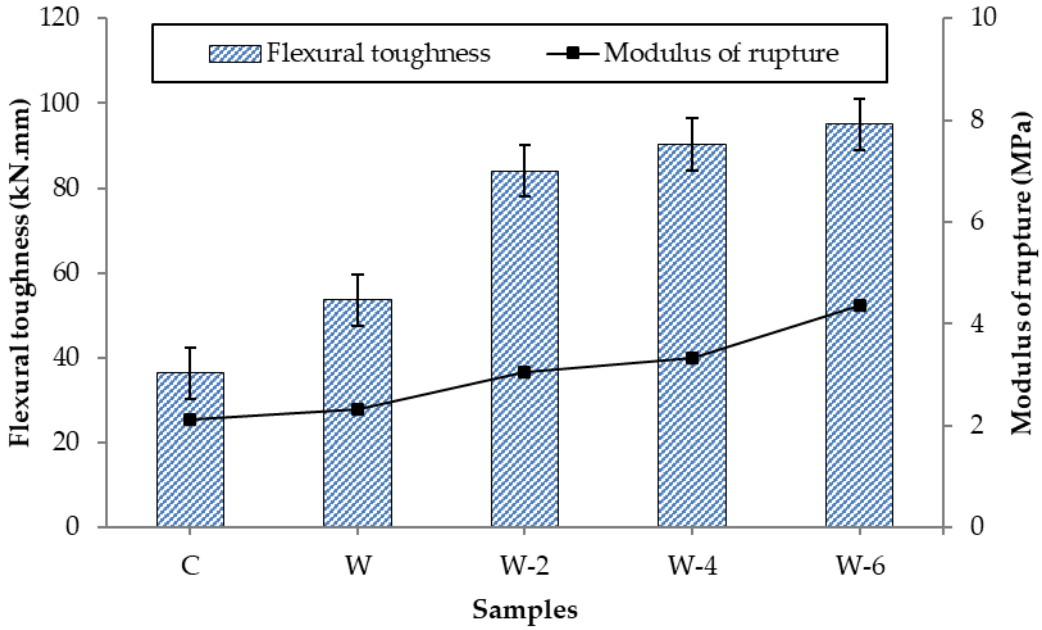

Figure 12. Dependence of modulus of rupture on toughness in control mix and FRCs.

3.5. Fracture Energy and Ductility Index

The monotonic increase in toughness with fiber content and the higher residual capacities at L/600 and L/150 (Table 10), together with the absence of visible fiber balling on fracture surfaces, indicate that the fiber dispersion was adequate with the tested dosages.

The G_f (fracture energy) and DI (ductility index) are fundamental descriptors of FRCs' post-cracking behavior and their ability to absorb energy during flexure. The DI indicates the ability of the material to undergo significant deformation beyond the elastic limit without a sudden failure while the G_f reflects the total energy absorbed by the specimen until a specified deflection limit. Understanding the relationship between these parameters is essential for evaluating the effectiveness of fiber reinforcement in enhancing the toughness

and deformation capacity of concrete. In this section, the interaction between the G_f and DI is examined based on the experimental results of beam specimens incorporating mine tailings and various dosages of waste tire wire fibers. The influence of increasing the fiber content on both the G_f and DI is also discussed in detail, providing insights into the overall flexural performance and failure characteristics of the composites. The variations in the G_f and DI due to fiber content are shown in Figure 13.

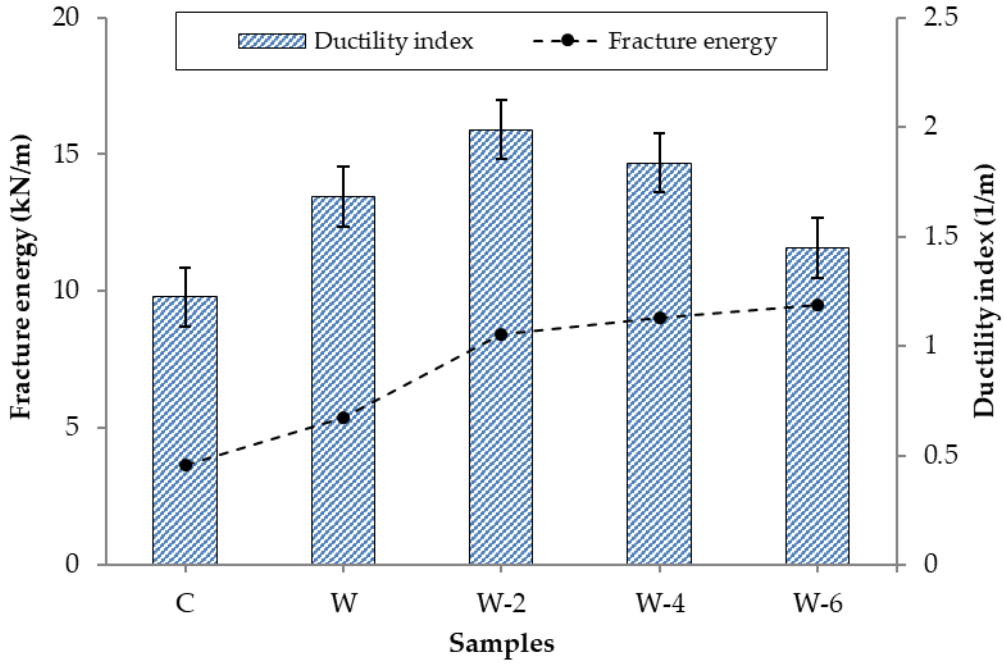

Figure 13. Changes in fracture energy and ductility index due to fiber content.

The G_f and DI improved significantly with the addition of fibers compared to the control mix, as shown in the Figure 13. The G_f increased steadily from approximately 3600 N/m in the control mix to over 9400 kN/m in the W-6 sample, an increase of more than 161%. A similar trend was observed in the DI, which rose from 1.22 in C to a peak value of approximately 1.95 in the W-2 mixture, corresponding to an increase of about 60%. However, the DI declined beyond a fiber dosage of 0.2% while the fracture energy continued to increase slightly with higher fiber contents. This suggests that although the fibers enhanced energy absorption, an excessive fiber content may lead to reduced deformability due to increased matrix stiffness or fiber agglomeration. These findings highlight the importance of optimizing the fiber dosage to achieve a balanced enhancement in both energy dissipation and ductility. The observed trend of increasing fracture energy (up to ~161%) accompanied by a peak in the DI (rising until a fiber dosage of 0.2% and slightly decreasing thereafter) aligns closely with the findings of recent studies. Khan et al. reported a 56–70% enhancement in G_f and substantial improvements in post-cracking ductility with the use of aligned hooked-end SFs [76]. Similarly, Wang et al. demonstrated that increasing the SF content from 0 to 2% produced linear increases in G_f, toughness, and ductility metrics [77]. Additionally, Hosen et al. documented dramatic DI improvements (up to 568% for energy ductility), reinforcing the critical interdependence between fiber dosage, energy absorption capacity, and ductile response in fiber-reinforced concrete composites [78]. Su et al. and Jin et al. highlighted that while increasing fiber dosage improves fracture resistance and energy absorption, it can also result in reduced ductility if the fiber content surpasses an optimal threshold [79,80]. Xu et al. similarly emphasized the role of fiber volume and orientation in enhancing fracture energy while maintaining a balanced post-cracking behavior in fiber-reinforced concrete composites [81].

Although the fracture energy G_f and toughness $U_{0\to L/150}$ increased monotonically with fiber content, the ductility index (DI) peaked at 0.2% (W-2 ≈ 1.99) and then declined at 0.4–0.6% (W-4 ≈ 1.84, W-6 ≈ 1.45) (Table 10). Two complementary factors explain this behavior. First, the DI used here is a normalized metric (proportional to G_f/P_{max}); therefore, large increases in peak load at higher fiber contents can mathematically lower the DI even when the absolute energy absorption is increasing. Second, at higher recycled tire steel fiber (RSF) dosages, dispersion challenges (local clustering, increased ITZ volume, and orientation bias under casting/three-point bending) can reduce post-peak deformability (i.e., steeper softening), even as the number of engaged fibers increases the energy dissipated by pull-out. Prior studies reported that excess steel fibers can cause clustering, locally weaken the interface and alter the softening branch; several works identified an optimum fiber volume beyond which the ductility or tensile indices no longer improved or may decrease despite gains in strength/toughness. These trends have been documented for SFRC/RSF systems and are tied to fiber type, geometry, dispersion quality, and the measurement window in ASTM C1609 [37]. Gao et al. linked fiber clustering at high dosages to degraded bond and altered cyclic responses [82]. Al Rifai et al. noted that beyond an optimal content, fibers may clump, creating weak spots and reducing tensile/flexural indices [83]. Mehmandari et al. showed RSF-based hybrid FRC's post-cracking response is highly dispersion-sensitive [65]. Fracture-mechanics analyses (e.g., updated bridged-crack models) captured how changes in pull-out vs. rupture balance reshape post-peak ductility. Test-method comparisons emphasized how ASTM C1609 [37] index definitions and evaluation windows affect perceived ductility. Our observations (rising G_f and higher residual capacities but lower DI at ≥0.4% RSF) are consistent with this body of evidence for non-monotonic ductility at elevated fiber volume fractions.

4. Conclusions

This study investigated the mechanical performance and sustainability potential of fiber-reinforced concrete incorporating mine tailings as the fine aggregate and waste tire wire as the reinforcing fiber. Based on the experimental results, the principal conclusions are as follows:

(1) The partial replacement of natural sand with mine tailings slightly increased the porosity and water absorption at early ages. However, the inclusion of waste tire wire at dosages of 0.4% and 0.6% significantly reduced these values at 28 days, indicating enhanced reduced permeability. This improvement supports the development of more durable concrete composites.

(2) The compressive strength of the mixtures progressively improved with increasing fiber content, reaching up to 26.0 MPa with the W-6 mix, an 18.2% increase compared to the control mix. Likewise, the splitting tensile strength improved by up to 7.1%, especially in the higher fiber content mixes due to effective fiber reinforcement by the tire wires.

(3) The waste tire wire significantly enhanced the flexural performance and toughness of the concrete. The modulus of rupture in the W-6 sample increased by 104% and the flexural toughness improved by 161% compared to the control mix. The load drop percentage decreased with higher fiber contents, indicating superior post-cracking behavior.

(4) The concrete specimens incorporating waste tire wire, particularly the W-6 sample with a 0.6% fiber content, exhibited significantly superior performance in terms of flexural load and deflection capacity, enhancing the concrete's ductility and energy absorption capability.

(5) The fracture energy steadily increased from 3.6 to 9.4 kN/m with rising fiber dosage. The ductility index peaked at a fiber content of 0.2% and declined slightly at higher dosages. This behavior emphasizes the importance of optimizing the fiber dosage to balance toughness and deformability as excessive fiber addition may lead to agglomeration and stiffness loss.

(6) The joint incorporation of mine tailings and recycled tire wire offers an effective, resource-efficient solution, simultaneously reducing virgin resource input and converting industrial waste into valuable materials, which align with circular economy and low-carbon goals.

In summary, the synergistic incorporation of mine tailings and waste tire wire significantly improved the mechanical, durability, and post-cracking properties of concrete. These results confirm the feasibility of producing structurally efficient and environmentally responsible concrete by revalorizing two major industrial waste streams. Future work could focus on the hybridization of recycled tire wire with other industrial fibers to further enhance composite performance. Moreover, long-term durability aspects, including freeze–thaw, chloride penetration, and sulfate attack resistance, should be investigated to validate the field performance of such concretes. In addition, life-cycle assessments (LCAs) and cost–benefit analyses could provide deeper insights into the broader sustainability potential of incorporating mine tailings and recycled tire wire into concrete production.

Author Contributions: Conceptualization, M.T.S., Y.S.A., and A.G.S.; methodology, M.T.S.; investigation, Y.S.A.; resources, M.T.S. and A.G.S.; writing—original draft preparation, Y.S.A.; writing—review and editing, M.T.S. and Y.S.A.; visualization, M.T.S.; supervision, M.T.S.; project administration, M.T.S. All authors have read and agreed to the published version of the manuscript.

Funding: This research received no external funding.

Institutional Review Board Statement: Not applicable.

Informed Consent Statement: Not applicable.

Data Availability Statement: All data generated or analyzed during this study are included in this published article.

Conflicts of Interest: The authors declare no conflicts of interest.

References

1. Al-Kheetan, M.J. Properties of lightweight pedestrian paving blocks incorporating wheat straw: Micro-to macro-scale investigation. *Results Eng.* **2022**, *16*, 100758. [CrossRef]
2. Koucham, M.; Khalil, A.; Mouhagir, L.; Zouhri, L.; El Adnani, M. Comprehensive assessment of environmental behavior of mine tailings for sustainable waste management and mitigation of pollution risks. *Water* **2025**, *17*, 43. [CrossRef]
3. Akaryalı, E. Geochemical, fluid inclusion and isotopic (O, H and S) constraints on the origin of Pb–Zn±Au vein-type mineralizations in the Eastern Pontides Orogenic Belt (NE Turkey). *Ore Geol. Rev.* **2016**, *74*, 1–14. [CrossRef]
4. Çullu, M. Investigation of the mechanical and physical properties of concrete produced with lead–zinc mine waste rock. *Polytech. J.* **2018**, *21*, 427–435. [CrossRef]
5. El Machi, A.; El Berdai, Y.; Mabroum, S.; Safhi, A.e.M.; Taha, Y.; Benzaazoua, M.; Hakkou, R. Recycling of mine wastes in the concrete industry: A review. *Buildings* **2024**, *14*, 1508. [CrossRef]
6. Nandi, S.; Ransinchung, G.; Rana, G.B. A sustainable approach towards reducing cement consumption in the road sector using zinc industry waste. *Int. J. Pavement Res. Technol.* **2022**, *15*, 1463–1483. [CrossRef]
7. Amrani, M.; Taha, Y.; El Haloui, Y.; Benzaazoua, M.; Hakkou, R. Sustainable reuse of coal mine waste: Experimental and economic assessments for embankments and pavement layer applications in Morocco. *Minerals* **2020**, *10*, 851. [CrossRef]
8. Kotan, T.; Ardahanlı, M.; Özbey, Ö.F. Investigation of the fresh and mechanical properties of self-compacting concrete incorporating waste zinc slag powder. *Konya J. Eng. Sci.* **2023**, *11*, 518–529. [CrossRef]
9. Soutsos, M.N.; Le, T.T.; Lampropoulos, A.P. Flexural performance of fibre reinforced concrete made with steel and synthetic fibres. *Constr. Build. Mater.* **2012**, *36*, 704–710. [CrossRef]

10. Su, P.; Li, M.; Dai, Q.; Wang, J. Mechanical and durability performance of concrete with recycled tire steel fibers. *Constr. Build. Mater.* **2023**, *394*, 132287. [CrossRef]
11. Samindi, S.M.; Samarakoon, M.K.; Ruben, P.; Pedersen, J.W.; Evangelista, L. Mechanical performance of concrete made of steel fibers from tire waste. *Case Stud. Constr. Mater.* **2019**, *11*, e00259. [CrossRef]
12. Centonze, G.; Leone, M.; Aiello, M.A. Steel fibers from waste tires as reinforcement in concrete: A mechanical characterization. *Constr. Build. Mater.* **2012**, *36*, 46–52. [CrossRef]
13. Zeybek, Ö.; Özkılıç, Y.O.; Çelik, A.İ.; Deifalla, A.F.; Ahmad, M.; Sabri, M.M. Performance evaluation of fiber-reinforced concrete produced with steel fibers extracted from waste tire. *Front. Mater.* **2022**, *9*, 1057128. [CrossRef]
14. Mindess, S.; Young, J.F.; Darwin, D. *Concrete*, 2nd ed.; Pearson Education Inc., Prentice Hall: Saddle River, NJ, USA, 2002; p. 629.
15. Ige, O.E.; Olanrewaju, O.A.; Duffy, K.J.; Collins, O.C. Environmental Impact Analysis of Portland Cement (CEM1) Using the Midpoint Method. *Energies* **2022**, *15*, 2708. [CrossRef]
16. Neupane, R.P.; Devi, N.R.; Imjai, T.; Rajput, A.; Noguchi, T. Cutting-edge techniques and environmental insights in recycled concrete aggregate production: A comprehensive review. *Resour. Conserv. Recycl. Adv.* **2025**, *25*, 200241. [CrossRef]
17. Rahman, Z.; Khan, M.; Hussain, M. A study on concrete with waste rubber tyre as partial replacement to coarse aggregate. *Int. J. Eng. Res. Technol. (IJERT)* **2017**, *6*, 234–237.
18. Xiaoyan, H.; Li, W.; Aijiu, C.; Lingyun, F.; Yanting, J.; Zhihao, W.; Zhenzan, G.; Keliang, L.; Qun, Y.; Xiaozhou, X.; et al. Experimental and analytical evaluation of mechanical properties of rubberized concrete incorporating waste tire crumb rubber. *Case Stud. Constr. Mater.* **2025**, *23*, e04970. [CrossRef]
19. Tate, S.M.; Hamid, H.F.; Durham, S.A.; Chorzepa, M.G. Investigation into recycled rubber aggregates and steel wire fiber for use in concrete subjected to impact loading. *Infrastructures* **2020**, *5*, 82. [CrossRef]
20. Liu, H.; Duan, H.; Gao, H.; Wang, Z.; Zhang, J. Graphite tailings' effects on mechanical and physical properties of eco-efficient steel fiber-reinforced concrete. *Buildings* **2022**, *12*, 509. [CrossRef]
21. Gayana, B.C.; Chandar, K.R. Sustainable use of mine waste and tailings with suitable admixture as aggregates in concrete pavements-A review. *Adv. Concr. Constr.* **2018**, *6*, 221–243. [CrossRef]
22. Amjad, H.; Abd-Elaal, E.S.; Ma, X.; Benn, T.; Fisher, M. A critical review of iron ore tailings as cement and aggregate substitutes for robust infrastructure: Mechanical, durability, eco-economic, and social impacts. *J. Clean. Prod.* **2025**, *492*, 144853. [CrossRef]
23. Karthikeyan, B.; Kathyayini, R.; Kumar, V.A.; Uthra, V.; Kumaran, S.S. Effect of dumped iron ore tailing waste as fine aggregate with steel and basalt fibre in improving the performance of concrete. *Mater. Today Proc.* **2021**, *46*, 7624–7632. [CrossRef]
24. Gao, H.; An, B.; Dai, Y.; Fan, K.; Ding, J.; Liu, H. Utilizing of graphite tailings as fine aggregates in asphalt mixture: Road performance and economic environment assessments. *Case Stud. Constr. Mater.* **2025**, *22*, e04807. [CrossRef]
25. Indian Institute of Technology Bombay (IITB). *Understanding RubCrete: How Waste Tyres Are Making Concrete Tougher and Greener*; IITB Research Highlights; Indian Institute of Technology Bombay (IITB): Mumbai, India, 2025.
26. Adıgüzel, D.; Tüylü, S.; Eker, H. Utilization of tailings in concrete products: A review. *Constr. Build. Mater.* **2022**, *360*, 129574. [CrossRef]
27. Zia, A.; Zhang, P.; Holly, I. Experimental investigation of raw steel fibers derived from waste tires for sustainable concrete. *Constr. Build. Mater.* **2023**, *368*, 130410. [CrossRef]
28. Fares, G.; Alsaif, A.; Alhozaimy, A. Hybridization and cost-performance analysis of waste tire steel fibers into high-volume powdered scoria rocks-based ultra-high performance concrete. *J. Build. Eng.* **2023**, *72*, 106568. [CrossRef]
29. Mobasher, B.; Cheng, Y.L. Effect of interfacial properties on the crack propagation in cementitious composites. *Adv. Cem. Based Mater.* **1996**, *4*, 93–105. [CrossRef]
30. Gao, J.; Sun, W.; Morino, K. Mechanical properties of steel fiber-reinforced, high-strength, lightweight concrete. *Cem. Concr. Compos.* **1997**, *19*, 307–313. [CrossRef]
31. Yazıcı, Ş.; İnan, G.; Tabak, V. Effect of aspect ratio and volume fraction of steel fiber on the mechanical properties of SFRC. *Constr. Build. Mater.* **2007**, *21*, 1250–1253. [CrossRef]
32. Wu, Z.; Shi, C.; He, W.; Wu, L. Effects of steel fiber content and shape on mechanical properties of ultra high performance concrete. *Constr. Build. Mater.* **2016**, *103*, 8–14. [CrossRef]
33. *ASTM C642*; Standard Test Method for Density, Absorption, and Voids in Hardened Concrete. ASTM International: West Conshohocken, PA, USA, 2004.
34. *BS EN 12390-3*; Testing Hardened Concrete—Part 3: Compressive Strength of Test Specimens. British Standards Institution: London, UK, 2009.
35. *ASTM C39*; Standard Test Method for Compressive Strength of Cylindrical Concrete Specimens. ASTM International: West Conshohocken, PA, USA, 2021.
36. *ASTM C496*; Standard Test Method for Splitting Tensile Strength of Cylindrical Concrete Specimens. ASTM International: West Conshohocken, PA, USA, 2017.

37. *ASTM C1609*; Standard Test Method for Flexural Performance of Fiber-Reinforced Concrete (Using Beam with Third-Point Loading). ASTM International: West Conshohocken, PA, USA, 2019.
38. Noushini, A.; Hastings, M.; Castel, A.; Aslani, F. Mechanical and flexural performance of synthetic fibre reinforced geopolymer concrete. *Constr. Build. Mater.* **2018**, *186*, 454–475. [CrossRef]
39. Aksüt, Y.S.; Çullu, M.; Yetgin, Ş. Optimal ratio of steel and polyester fibers on the mechanical behavior of alkali-activated concrete produced by industrial waste minerals. *Iran J. Sci. Technol. Trans. Civ. Eng.* **2024**, *49*, 657–671. [CrossRef]
40. Johansson, L.; Bahrami, A.; Wallhagen, M.; Cehlin, M. A comprehensive review on properties of tailings-based low-carbon concrete: Mechanical, environmental, and toxicological performances. *Dev. Built Environ.* **2024**, *18*, 100428. [CrossRef]
41. Saedi, A.; Jamshidi-Zanjani, A.; Darban, A.K.; Mohseni, M.; Nejati, H. Utilization of lead–zinc mine tailings as cement substitutes in concrete construction: Effect of sulfide content. *J. Build. Eng.* **2022**, *57*, 104865. [CrossRef]
42. Roshan, N.; Ghalehnovi, M. The effect of recycled-tire steel fiber and engineered steel fiber on rebar corrosion and shear behavior of corroded RC beam. *Case Stud. Constr. Mater.* **2023**, *19*, e02251. [CrossRef]
43. Manan, A.; Zhang, P.; Alattyih, W.; Alzara, M.; Ahmad, J.; Yosri, A.M. Physical properties of recycled concrete powder and waste tyre fibre reinforced concrete. *Proc. Inst. Civ. Eng. Eng. Sustain.* **2024**, *178*, 171–184. [CrossRef]
44. Wang, J.; Zhao, C.; Li, Q.; Song, G.; Hu, Y. The synergistic effect of recycled steel fibers and rubber aggregates from waste tires on the basic properties, drying shrinkage, and pore structures of cement concrete. *Constr. Build. Mater.* **2025**, *470*, 140574. [CrossRef]
45. Soulioti, D.V.; Barkoula, N.M.; Paipetis, A.; Matikas, T.E. Effects of fibre geometry and volume fraction on the flexural behaviour of steel-fibre reinforced concrete. *Strain* **2011**, *47*, e535–e541. [CrossRef]
46. Şimsek, O. *Concrete and Concrete Technology*, 6th ed.; Seçkin Publishing House: Ankara, Turkey, 2020.
47. Aswathi, R.; Shahla, C.P. Mechanical properties of hybrid fiber reinforced geopolymer concrete. *Int. Res. J. Eng. Technol.* **2019**, *6*, 170–173. Available online: https://www.irjet.net/archives/V6/i8/IRJET-V6I830.pdf (accessed on 16 August 2025).
48. Venkateswarlu, M.; Gunneswara Rao, T.D. Effect of steel and PVA fibres as monofibres on strength and cracking properties of fly ash and slag-based alkali-activated concrete. *J. Eng. Appl. Sci.* **2023**, *70*, 100. [CrossRef]
49. Tokyay, M.; Ramyar, K.; Turanlı, L. Behavior of polypropylene and steel fiber high strength concrete under compressive and tensile loads. In Proceedings of the TMMOB Chamber of Civil Engineers 2nd National Concrete Congress Proceedings, Ankara, Turkey, 27–30 May 1991; pp. 303–311.
50. Kolesnikov, G.; Shekov, V.; Gavrilov, T. Modeling the influence of non-constant Poisson's ratio on crack formation under uniaxial compression of rocks and concrete. *Eng* **2025**, *6*, 130. [CrossRef]
51. Bankir, Ş.; Bikce, M. Experimental investigation and statistical evaluation of the effects of steel fiber aspect ratio and fiber rate on static and dynamic mechanical properties of concrete. *Constr. Build. Mater.* **2024**, *414*, 135064. [CrossRef]
52. Shadfar, A.; Nani, M.; Shirinabadi, R.; Hosseini, S.A. The feasibility of constructing rubber concrete pavement reinforced with recycled and industrial steel fibers. *Results Mater.* **2025**, *25*, 100657. [CrossRef]
53. Zia, A.; Zhang, P.; Holly, I.; Prokop, J. Sustainability enhancement through high-dose recycled tire steel fibers in concrete: Experimental insights and practical applications. *Sustainability* **2023**, *15*, 15760. [CrossRef]
54. Gong, J.; Ma, Y.; Fu, J.; Hu, J.; Ouyang, X.; Zhang, Z.; Wang, H. Utilization of fibers in ultra high-performance concrete: A review. *Compos. Part B Eng.* **2022**, *241*, 109995. [CrossRef]
55. Dziomdziora, P.; Smarzewski, P. Effect of hybrid fiber compositions on mechanical properties and durability of ultra-high-performance concrete: A comprehensive review. *Materials* **2025**, *18*, 2426. [CrossRef] [PubMed]
56. Oyejobi, D.O.; Firoozi, A.A.; Fernández, D.B.; Avudaiappan, S. Integrating circular economy principles into concrete technology: Enhancing sustainability through industrial waste utilization. *Results Eng.* **2024**, *24*, 102846. [CrossRef]
57. *EN 13877-1:2023*; Concrete Pavements—Part 1: Materials. CEN—European Committee for Standardization: Brussels, Belgium, 2023.
58. *ACI 325.9 R*; Guide for Construction of Concrete Pavements and Concrete Bases. American Concrete Institute (ACI): Farmington Hills, MI, USA, 2015.
59. Köksal, F.; Beycioğlu, A.; Dobiszewska, M. Optimization based on toughness and splitting tensile strength of steel-fiber-reinforced concrete incorporating silica fume using response surface method. *Materials* **2022**, *15*, 6218. [CrossRef]
60. Cui, D.; Wang, L.; Zhang, C.; Xue, H.; Gao, D.; Chen, F. Dynamic splitting performance and energy dissipation of fiber-reinforced concrete under impact loading. *Materials* **2024**, *17*, 421. [CrossRef]
61. Almohammed, F.; Thakur, M.S.; Lee, D.; Kumar, R.; Singh, T. Flexural and split tensile strength of concrete with basalt fiber: An experimental and computational analysis. *Constr. Build. Mater.* **2024**, *414*, 134936. [CrossRef]
62. Sukontasukkul, P. Tensile behaviour of hybrid fibre reinforced concrete. *Adv. Cem. Res.* **2004**, *16*, 115–122. [CrossRef]
63. Sukontasukkul, P.; Pongsopha, P.; Chindaprasirt, P.; Songpiriyakij, S. Flexural performance and toughness of hybrid steel and polypropylene fibre reinforced geopolymer. *Constr. Build. Mater.* **2018**, *161*, 37–44. [CrossRef]
64. Maldar, M.; Kianoush, R.; Siad, H.; Lachemi, M. An experimental investigation on the mechanical performance of engineered cementitious composites with different types of steel fiber. *Materials* **2025**, *18*, 2990. [CrossRef] [PubMed]

65. Mehmandari, T.A.; Shokouhian, M.; Josheghan, M.Z.; Mirjafari, S.A.; Fahimifar, A.; Armaghani, D.J.; Tee, K.F. Flexural properties of fiber-reinforced concrete using hybrid recycled steel fibers and manufactured steel fibers. *J. Build. Eng.* **2024**, *98*, 111069. [CrossRef]
66. Bzeni, D.K. Investigating the influence of fiber content and geometry on the flexural response of fiber-reinforced cementitious composites. *J. Compos. Sci.* **2024**, *8*, 347. [CrossRef]
67. He, J.; Sun, C.; Wang, X. Mechanical properties and microanalytical study of concrete reinforced with blended corn straw and scrap steel fibers. *Materials* **2024**, *17*, 3844. [CrossRef]
68. Aksoylu, C.; Özkılıç, Y.O.; Hadzima-Nyarko, M.; Işık, E.; Arslan, M.H. Investigation on improvement in shear performance of reinforced-concrete beams produced with recycled steel wires from waste tires. *Sustainability* **2022**, *14*, 13360. [CrossRef]
69. Sanok, A.; Domski, J.; Kobaka, J.; Logoń, D. Torsional behavior of waste fiber-reinforced concrete. *Materials* **2024**, *17*, 3269. [CrossRef]
70. Suárez González, J.; Lopez Boadella, I.; López Gayarre, F.; López-Colina Pérez, C.; Serrano López, M.; Stochino, F. Use of mining waste to produce ultra-high-performance fibre-reinforced concrete. *Materials* **2020**, *13*, 2457. [CrossRef]
71. Jiang, M.; Cao, S.; Yilmaz, E. Enhanced strength and fracture features of tailings-based concrete reinforced with fibers and X-shaped rocks. *J. Mater. Res. Technol.* **2025**, *36*, 62–71. [CrossRef]
72. Zaid, O.; Ahmed, M.; Yosri, A.M.; Alshammari, T.O. Evaluating the impact of mine tailings wastes on the development of sustainable ultra-high performance fiber reinforced concrete. *Sci. Rep.* **2025**, *15*, 6285. [CrossRef]
73. Yu, J.; Wu, Q.; Zhao, D.; Jiao, Y. Influence of recycled tire steel fiber content on the mechanical properties and fracture characteristics of ultra-high-performance concrete. *Materials* **2025**, *18*, 3300. [CrossRef] [PubMed]
74. Wu, L.; Feng, C.; Qiu, J.; Wang, L.; Peng, Y.; Liu, J. Influence of recycled tire steel fibers on the mechanical properties and carbon emissions of high-performance cement-based materials. *Materials* **2025**, *18*, 3008. [CrossRef] [PubMed]
75. Yan, C.; Jiang, C.; Zhang, J.; Li, L.; Li, G. Experimental study on flexural performance of recycled aggregate concrete with recycled tire steel fiber. *Buildings* **2023**, *13*, 3046. [CrossRef]
76. Khan, S.; Qing, L.; Ahmad, I.; Mu, R.; Bi, M. Investigation on fracture behavior of cementitious composites reinforced with aligned hooked-end steel fibers. *Materials* **2022**, *15*, 542. [CrossRef]
77. Wang, Z.; Gou, J.; Gao, D. Experimental study on the fracture parameters of concrete. *Materials* **2021**, *14*, 129. [CrossRef]
78. Hosen, M.A.; Liew, K.M.; Lee, H.K. Ductility enhancement of sustainable fibrous-reinforced high-strength lightweight concrete. *Polymers* **2022**, *14*, 727. [CrossRef]
79. Su, J.Y.; Luo, R.H.; Chen, Z.B.; Lin, J.X.; Huang, P.Y.; Guo, Y.C. Experimental study on the fracture performance of rubberized high strength-high ductility concrete with J-integral method. *Constr. Build. Mater.* **2024**, *421*, 135668. [CrossRef]
80. Jin, A.H.; Woo, J.S.; Yun, H.D.; Kim, S.W.; Park, W.S.; Choi, W.C. Influence of concrete strength and fiber properties on residual flexural strength of steel fiber-reinforced concrete. *Constr. Build. Mater.* **2025**, *489*, 142366. [CrossRef]
81. Xu, W.; Chen, Y.; Miao, H.; Zhang, L. An experimental study on fracture characteristics of high-performance fiber-reinforced cement composites through combined acoustic emission and digital image correlation. *J. Build. Eng.* **2025**, *103*, 112110. [CrossRef]
82. Gao, D.; Gu, Z.; Wei, C.; Wu, C.; Pang, Y. Effects of fiber clustering on fatigue behavior of steel fiber reinforced concrete beams. *Constr. Build. Mater.* **2021**, *301*, 124070. [CrossRef]
83. Al Rifai, M.M.; Sikora, K.S.; Hadi, M.N.S. Effect of micro steel fibers volume fraction on behavior of high-strength self-compacting concrete. *Constr. Build. Mater.* **2024**, *450*, 138709. [CrossRef]